IMPERFECTION EVALUATION METHODS OF LARGE SCALE SPIRAL-WELDED TUBES BASED ON EXPERIMENTAL TESTS AND PROGRESSIVE REVERSE ENGINEERING PROCEDURES

ANDREAS MÜLLER[1,3], TILL TÖPPERWIEN[2] and ANDREAS TARAS[3]

[1]*Institute of Structural Engineering, Bundeswehr University Munich, Munich, Germany.*
E-mail: andreas.mueller@unibw.de
[2]*University of Applied Science Munich, Munich, Germany.*
[3] *Institute of Structural Engineering, Chair of Steel and Composite Structures, ETH Zurich, Switzerland*

Spiral welded tubes of large diameter are commonly used in the pipeline industry, in applications for combiwalls, very slender (D/t > 300) wind turbine towers, and - more recently - in the construction of gas-insulated transmission lines (GIL), where these tubes are used as enclosures. Depending on the application, some load scenarios lead to significant compression and bending forces. With higher steel grades, this type of structure becomes strongly sensitive to geometric imperfections – caused by the manufacturing process of de-coiling, cold forming and welding into a continuous tube - and local buckling is predicted to be the critical design criteria. However, international shell structure design rules for cylindrical shells were not derived for spiral welded tubes and the existing validation is limited. A key difference to other imperfection shapes is given by the influence of the angle between spiral weld and the direction of stress. This paper is based on 17 experimental tests that were conducted on spiral welded aluminium tubes (D/t = 60) with and without girth welds in order to investigate their load bearing and deformation capacity in compression. Additionally, full body 3D scans were made to observe imperfections around welds and the overall ovalization of the tubes as well as to create numerical models based on the real specimen geometry by using progressive reverse engineering methods. A variety of factors, such as the spiral weld gradient, the imperfection amplitude, the tube length and the slenderness, have an influence on the buckling and post-buckling behavior as well as the deformation capacity of such components. The proposed paper presents a detailed look at the imperfections of spiral welded & orbital welded tubes and their evaluation.

Keywords: Spiral-welded tubes; Reverse engineering; Local buckling; Circular hollow sections; Weld inducted imperfections.

1 Introduction

In the authors' ongoing research efforts aimed at providing a consistent representation of strength and deformation capacities as a function of cross-sectional slenderness, it is planned to take account of the multitude of effects on the deformation capacity in tubular elements and structures, such as residual stresses, length-effects and – most significantly – initial imperfections in combination with different load cases. A recently conducted study by Müller (2019) – based on

Proceedings of the 17th International Symposium on Tubular Structures.
Editors: X.D. Qian and Y.S. Choo
Copyright © ISTS2019 Editors. All rights reserved.
Published by Research Publishing, Singapore.
ISBN: 978-981-11-0745-0; doi:10.3850/978-981-11-0745-0_098-cd

experimental test and proceeding of the RFCS funded project Hollosstab No. 709892, Toffolon (2019) – on the influence of different eigenmodes on the rotation capacity, especially the post buckling behavior, showed a slenderness dependent variety of the post-buckling paths of squared hollow sections (SHS). An additional comparative FEM evaluation of surface-scan-based real geometry models showed a variability in the post-buckling behavior of SHS and RHS hollow sections (Müller 2019). The results of this study led to a confirmation of the conclusions described e.g. by Boeraeve (1993), i.e. that the post buckling behavior and the plastic hinge rotation is strongly influenced by initial imperfection. Therefore, a thorough analysis on recently collected 3D-Scan data of spiral welded tubes was conducted to evaluate local imperfections provoked by spiral and orbital welds (also known as girth welds). Fundamental groundwork on which this study is based was provided by Ding (1996), Pircher (2001), Teng (2005) and Sadowski (2015).

2 Full-scale Experimental Tests and Results

2.1 *Test program – scope and setup*

The experimental investigation presented in this paper is part of two research projects on spiral welded tubes – described here as "test series 1" and "test series 2" – conducted in the laboratory of the Bundeswehr University Munich between September 2017 and July 2019. All tubes are made of material with the chemical designation AlMg4,5Mn0,7 H111 (technical designation: EN AW-5083, see Eurocode 9-1-1 (2007) with a nominal 0.2% offset yield strength between 105 MPa and 125 MPa.

Test series 1 consists of 9 spiral welded tubes with lengths of 2500 mm and the thickness of t = 8.5 mm. (specimen #001 - #009). All 9 specimens of test series 2 were slightly thinner with t = 7.5 mm but had the same length of 2500 mm and also an additional orbital weld (connection between two spiral welded tubes). The specimens varied partially in their geometrical features. Thus, some specimens had an open and welded inspection port, "precast" damages/buckles and an insufficient quality of the orbital welds. During the testing procedure all sections were subjected to centric compression in order to determine the load carrying capacity under pure pressure as well as the assessment of the post-buckling behavior and the overall deformation capacity. In addition, the effective imperfections of the real specimen geometry were determined by using an optical 3D digitizing system (Carl Zeiss Optotechnik GmbH). By means of further evaluations of the collected data, conclusions can be drawn about the existing imperfections of the spiral-welded tubes, see Section 3. In order to determine surface displacements on full scale specimens, as well as to verify the discrete displacement measurements, a Digital Image Correlation device (ARAMIS™ by GOM) was employed.

2.2 *Test results – elasto-plastic buckling loads*

The tested specimens of test series 1, which were all produced from the same coil and on the same machine, unsurprisingly had a quite similar load-bearing behavior, with very small differences in the maximum load-bearing capacity. The overall deviations were less than 3% with a mean maximum Force of F_{max} = 2688 kN and a mean displacement of D_{mean} = 26.4 mm. Because of the higher variety between the individual specimens of test series 2, outliers could not be avoided. Test specimen V05 e.g. was weakened by cutting out a round inspection hole which lead to a drop in the maximum force by 11% compared to the mean value of F_{max} = 1795 kN.

During the stub column test of test series 1 the dents exclusively appeared in the top or bottom area, never in the middle of the specimen. The buckling shape had either a diamond form or a so-called "elephant foot", in some cases even a combination of those two. However, this did not have any particular effects on the maximum buckling load capacity. The specimens of test series 2 showed a completely different behavior. The overall recognized assumption that orbital welds,

and consequently the imperfections resulting from them, are detrimental to thin shells loaded by pure compression and bending, can be confirmed after the test results of test series 2. All specimens showed the same behavior after reaching the maximum load by developing local buckles around the orbital weld while falling into the descending branch. As this buckling shape was by far the most damaging, it surpassed other influences like the precast indentation and the spiral weld imperfections.

3 Imperfection Measurement and Assessment

3.1 *Reverse engineering procedure*

The effective imperfections of the real specimen geometry were determined by using an optical 3D digitizing system that uses the Digital Image Correlation technique. This effort was made due to two main reasons: first, implementing the real specimen geometry into an FE based program to evaluate the laboratory tests; second, in order to derive a "typical" imperfection geometry for spiral welded tubes with and without a tube connecting orbital weld.

The general workflow procedure for the reverse engineering applications can be obtained from Fig. 1. The upper part of the workflow, which leads from a real scanned test specimen to a finite element-based model, was already tested and performed successfully by Müller (2017) and Toffolon (2019). However, a more detailed analysis of imperfection was never conducted as it was not the prior focus.

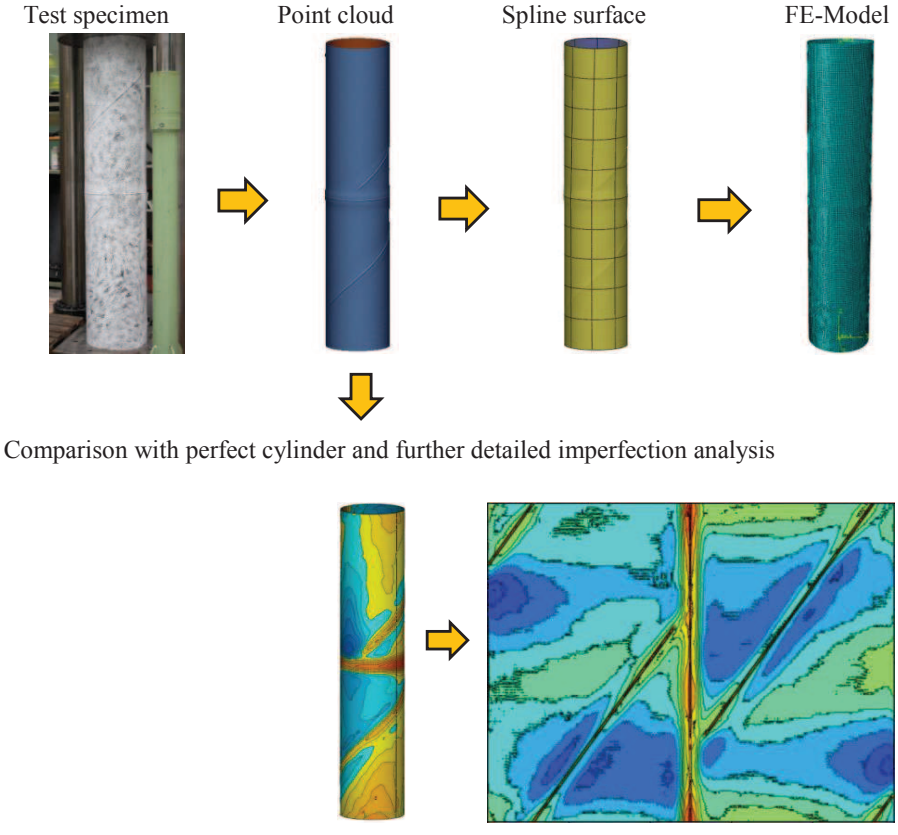

Figure 1. Applied reverse engineering work-flow scheme

3.2 *Imperfection evaluation – orbital weld*

Before looking at the imperfections in detail, the scanned data had first to be aligned and compared with the geometry of a perfect cylinder. These steps were conducted by using the commercial software Geomagic Design X and Geomagic Control X, respectively. The prepared data was then implemented into a python script developed at the Bundeswehr University Munich, Institute of Steel Structures. The imperfection data of each tested specimen was transformed to a flat surface by "unfolding" the cylinder. Using than the Python griddate command allows the implementation of a uniformly-spaced x(Height)-y(Circumference) grid (see Fig.2). Subsequently by applying a 1D full wave Fourier series it was possible to eliminate influences related to global sagging and ovalization (low harmonics k=0 – k=4, see Fig.3) along the circumferential direction, thus leveling the local weld imperfections.

$$w(x,y) = \sum_{k=0}^{K} \left(a_k(y) \cdot \cos\left(2 \cdot \pi \cdot k \cdot \frac{x}{x_{\max}} \right) + b_k(y) \cdot \sin\left(2 \cdot \pi \cdot k \cdot \frac{x}{x_{\max}} \right) \right) \tag{1}$$

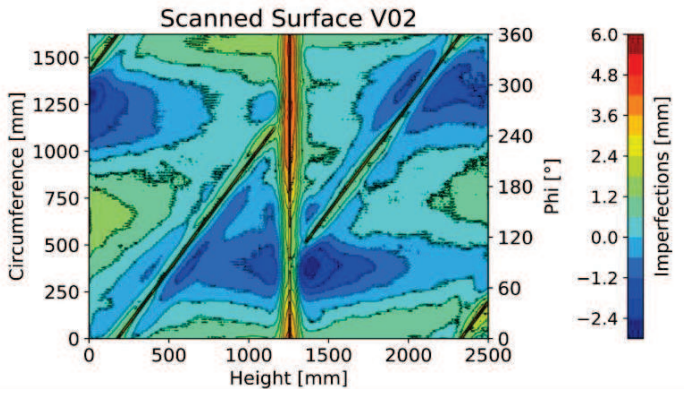

Figure 2. Contour plot of the raw scanned surface after gridding

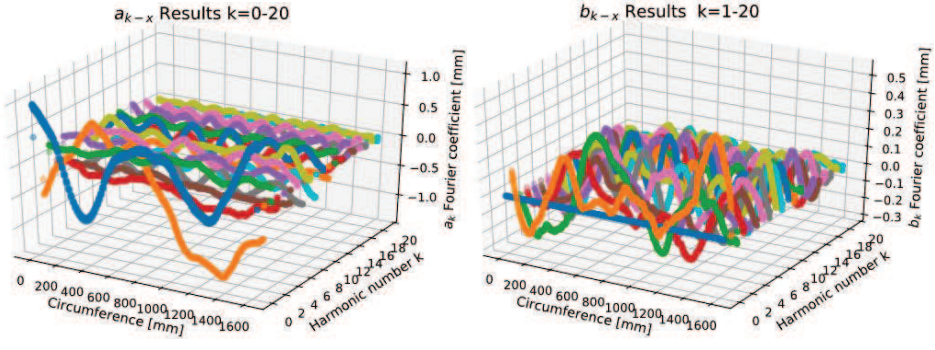

Figure 3. a_{k_x} and b_{k_x} Fourier coefficients up to k=20, specimen V02

By exclusively addressing high harmonics (see Fig.4) it was possible to eliminate imperfections associated with spiral welds (see Fig.5). As a result, an adjusted surface with just one orbital weld could be obtained. This procedure was executed for every specimen of test series 2, except specimen V10, to obtain a typical orbital imperfection form associated with this kind of manufacturing process (see Fig.6).

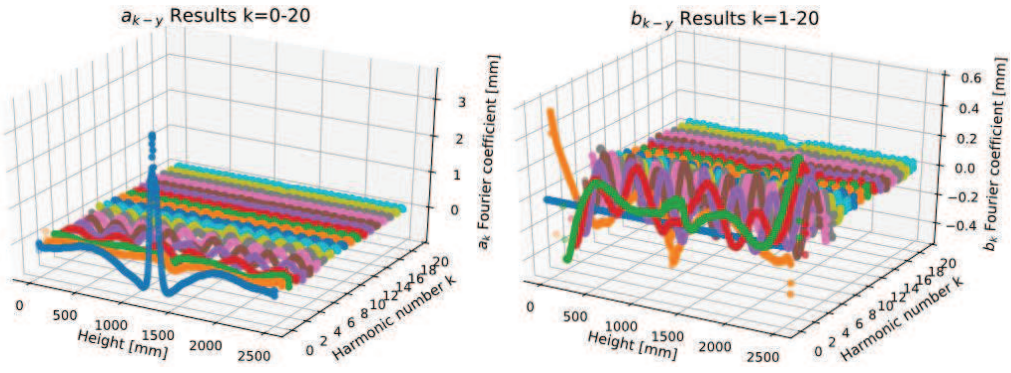

Figure 4. a_{k_y} and b_{k_y} Fourier coefficients up to k=20, specimen V02

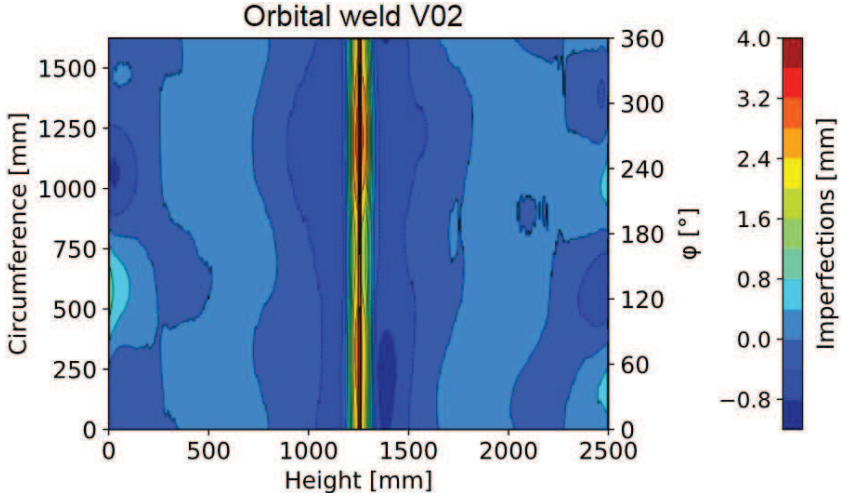

Figure. 5. Adjusted surface without the influence of ovalisation and spiral welds

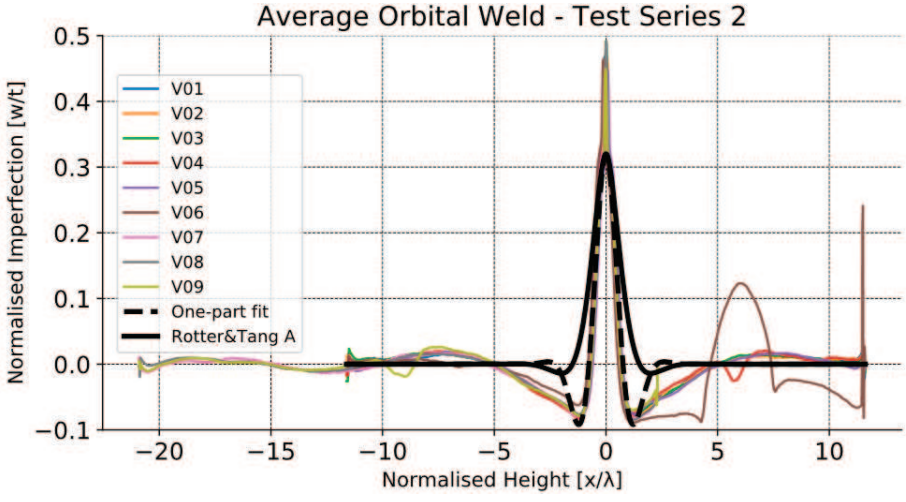

Figure 6. Extracted imperfection shapes V01 – V09, Orbital Weld

A widly used expression to describe imperfetion shapes is the type 'A' weld depression of Rotter & Teng (1989) (Eq. 2), where λ is the linear meridional bending half-wavelength and x_w the meridional location of the centre of a girth weld. This form has been adopted in numercical parametric studies (Sadowski 2015) and is widely considered as a particulary damaging imperfection for thin cylindrical shells under uniform axial compression and local bending. It was recently used in a demanding study on large spiral welded carbon steel tubes with good accordance describing the girth weld imperfections. However, using this imperfection form gives a rather inaccurate fitting result within the scope of the tested tubes presented in this study.

$$w(x) = \delta \cdot \left(\cos\left(\frac{\pi}{\lambda} \cdot \left| x - x_W \right| \right) + \sin\left(\frac{\pi}{\lambda} \cdot \left| x - x_W \right| \right) \right) \cdot \exp\left(\frac{\pi \left| x - x_W \right|}{\lambda} \right) \tag{2}$$

$$\lambda = \frac{\pi \cdot \sqrt{r \cdot t}}{\sqrt[4]{3 \cdot \left(1 - \nu^2\right)}} \tag{3}$$

The next attempt for a fitted imperfection shape was a one-part characterization, shown in the following equation. δ is the normalized imperfection amplitude. Parameters a, b, c and d were determined by a least-squares fitting procedure using the programming language python and the *scipy* library.

$$w(x) = \delta \cdot \cos\left(a \cdot \pi \left(\frac{\left| x - x_W \right|}{d\lambda} \right) \right) \cdot \exp\left(-b \cdot \left(\frac{\left| x - x_W \right|}{d\lambda} \right)^c \right) \tag{4}$$

By maximizing the mean coefficient of determination r^2 (Eq. 5) it was possible to create a best-fit imperfection shape using Equation 3, based on the full set of specimens of test series 2. The r^2 coefficient is defined as follows.

$$r^2 = 1 - \frac{SS_{err}}{SS_{tot}} \quad where \quad SS_{err} = \sum_{i=1}^{N} \left(y_i - f_i \right)^2 \quad and \quad SS_{tot} = \sum_{i=1}^{N} \left(y_i - \bar{y} \right)^2 \tag{5}$$

y_i and f_i are the i-th measured data point and the corresponding predicted value, respectively. N is the total amount of all data points and $\bar{y}$ the mean of the measured values. The constants in Eq. 4 were found to be a = 5.70, b = 32.65, c = 1.76 and d = 4.34 and a corresponding coefficient of r^2 = 0.86.

3.3 *Imperfection evaluation – spiral weld*

A similar but particularly efficient solving procedure as for the orbital weld was chosen for the evaluation of spiral welds. The scanned and mapped data had to be rotated around the helical weld angle first. Due to a shorter imperfection length of the spiral welds, caused by the automated, continuous fabrication technique, it was simpler to reduce the data around the welds and to eliminate the orbital weld. The elimination of the orbital weld was of course just necessary for the evaluation of test series 2, as test series 1 had only spiral welds. After these initial steps, again the python griddata function was used. By means of 1D Fourier Series expansion the ovalization was minimized. After leveling the local imperfections, a mean imperfection, representative for each considered imperfection area, was calculated.

A summary of the specimens of test series 1 and 2 that were taken into account is shown in Fig. 7. A one-part characterization was implemented first. The corresponding constants were

found to be a = 3.97, b = 76.78, c = 3.89 and d = 3.65 and the additional coefficient of determination $r^2 = 0.92$. By looking closely at the overall imperfection shape of the spiral welds, one can recognize an asymmetrical nature with the center around $\eta = 0$. A similar evaluation result was shown by Sadowski (2015). Therefore, an additional two-part characterization was attempted which describe the area to the right and to the left of the spiral weld separately by using an equal fitting technique as for the one-part representation. The constants for the two-part representation can be summarized for $\eta < 0$ with: $a_- = 51.18$, $b_- = 430.97$, $c_- = 1.56$, $d_- = 57.96$; for $\eta > 0$ with: $a_+ = 0.90$, $b_+ = 2.51e\text{-}04$, $c_+ = 0.64$, $d_+ = 3.15$, whereby dimension η describes the considered distance rectangular to the spiral weld. The coefficient of determination for the two-part approximation was calculated with $r^2 = 0.93$.

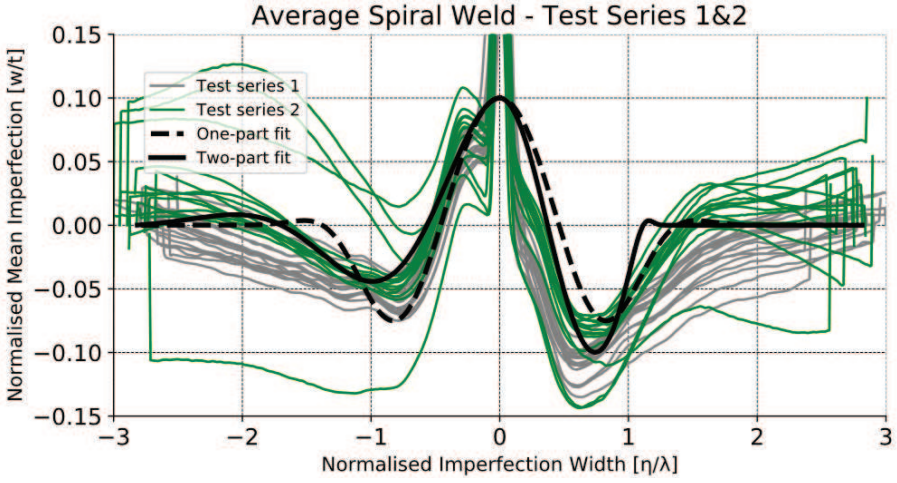

Figure 7. Extracted imperfection shapes of the spiral welds – Test series 1 & 2

4 Conclusions and Outlook

The presented paper describes a thorough analysis of imperfections caused by spiral and orbital welds in large scale cylindrical hollow sections. The evaluation based on 1D-Fourier series expansion showed reliable results. It was possible to take rather unusual imperfection patterns and separate these by calculating the range harmonic spectrum. By addressing low harmonics, effects like ovalization and sagging towards the circumferential direction could be reduced. This leads to a surface with leveled local imperfections. Hence the orbital as well as the spiral welded imperfections could be compared more accurately. Their characteristic shape was extracted and could be approximate by a one-part fit (orbital weld depression) and a two-part fit (spiral weld depression). An additional comparison with the Rotter and Teng A (1989) imperfection form led to an inaccurate fitting approach, as this form was established for thin-walled steel silos and tanks based on a different manufacturing process compared with the tubes presented in this paper. By first heating up the tubes and then pulling them onto a tube connecting ring of larger diameter the tubes are finally welded together. This process leads to longer imperfection length and higher amplitude compared to the weld induced imperfections which appear between the welded strakes of steel plates of thin steel silos. By looking at the code provisions of EN 1090-3 (2017), EC9-1-5 (2007) and EC3-1-6 (2017) regarding the imperfections, a mismatch is clearly visible by comparing the imperfection shape and its length of $l_{gx} = 4 \cdot \sqrt{r \cdot t}$.

First comparisons considering the scanned real geometry for geometrically and materially non-linear (GMNIA) calculations showed reliable results regarding the maximum force, displacement and even the buckling shape. However, an accurately scanned surface is not sufficient for accurate finite element-based modeling of imperfection sensitive members/structures. One may consider the case of a perfect cylinder of variable height with an additional orbital weld in the middle, whereby the orbital weld produces no initial imperfections as well as no heat affected zone in case of aluminum members. Taking only the scanned surface into account would lead to a model with an initial local imperfection in the middle of the specimen due to the weld bead and subsequently to inaccurate results regarding force and displacement. During further investigations on spiral-welded tubes, it is going to be necessary to implement the derived imperfections into FEM calculations, validating these results and transferring them to additional parametric studies (Müller 2018).

A further step towards a slenderness-based deformation and rotation capacity formulation is the expansion of the presented method in this paper on a wider range of tubular, hollow cross-sections, e.g. SHS, RHS and CHS profiles based on different manufacturing processes like cold-forming or hot rolling (preparing an imperfection database). Sadowski (2015) described that the critical terms in the harmonic analysis are usually not those with the largest amplitudes (typically low harmonics), but those with wavelengths close to that of the critical buckling mode (typically a high harmonic). Within this framework, the range of imperfections is going to be a not-negligible factor for the development of accurate predictor functions for the post-buckling paths.

References

Boeraeve, Ph., Lognard, B., Janss, J., Gérardy, J., Schleich, J. B., Elasto-plastic behaviour of steel frame works. Journal of Constructional Steel Research, Volume 27, Issues 1-3, 1993, pp. 3-21.

Ding, X., Coleman, R., Rotter, J. M., Techniques for precise measurement of large-scale silos and tanks, Journal of Surveying Engineering, 122(1), 14-25, February 1996

EN 1090-3, "Execution of steel structures and aluminium structures – Part 3: Technical requirements for aluminium structures", CEN – European Committee for Standardization, Brussels, 2017

EN 1993-1-6, "Eurocode 3. Design of steel structures – Part 1-6: Strength and stability of shell structures", CEN – European Committee for Standardization, Brussels, 2007 and 2017 versions.

EN 1999-1-1, "Eurocode 9. Design of aluminum structures – Part 1-1: General structural rules", CEN – European Committee for Standardization, Brussels, 2007

EN 1999-1-5, "Eurocode 9. Design of aluminum structures – Part 1-5: Shell structures", CEN – European Committee for Standardization, Brussels, 2007

Müller, A. Hausmann, B. Taras, A., Study on the influence of imperfections and strain hardening on the buckling strength of spiral –welded aluminum circular hollow sections. Conference paper, Eighth ICTWS 2018, 2018, Lisbon.

Müller, A., Taras A., On the post-buckling rotational capacity of squared hollow sections in uniform bending. An initial study on the impact of initial imperfections on deformation paths, Steel Construction – Design and Research 12, No. 3, 2019

Pircher, M., Berry, P. A., Ding, X., Bridge, R.Q., The shape of circumferential weld-inducted imperfections in thin-walled steel silos and tanks, Thin-Walled Structures 39, 999-1014, July 2001

Rotter, J.M., Teng, J.G., Elastic stability of cylindrical shells with weld depressions, Journal of Structural Engineering 115 (5), 1244-1263, 1989

Sadowski, A.J., Reinke, T., Van Es, S.H.J., Rotter, J.M.,Gresnigt, A.M., Ummenhofer, T., Harmonic analysis of measured initial geometric imperfections in large spiral welded carbon steel tubes, Engineering Structures, 85C, 234-248, January 2015

Toffolon, A., Taras, A., Development of an OIC.Type local buckling design approach for cold-formed unstiffened and groove-stiffened hollow sections, Thin-Walled Structures 144, June 2019

Teng, J.G., Lin, X., Rotter, J.M., Ding, X.L., Analysis of geometric imperfections in full-scale welded steel silos, Engineering Structures 27, 938-950, January 2005